THE JOURNAL OF BIOLOGICAL CHEMISTRY VOL. 289, NO. 39, pp. 27352–27362, September 26, 2014


# The Mitochondrial ADP/ATP Carrier Associates with the Inner Membrane Presequence Translocase in a Stoichiometric Manner*[S]

Received for publication, February 7, 2014, and in revised form, July 28, 2014 Published, JBC Papers in Press, August 14, 2014, DOI 10.1074/jbc.M114.556498

**Carola S. Mehnert[‡§1], Heike Rampelt[‡], Michael Gebert[‡§2], Silke Oeljeklaus[¶‖], Sandra G. Schrempp[‡§], Lioba Kochbeck[‡], Bernard Guiard[**], Bettina Warscheid[¶‖], and Martin van der Laan[‡‖3]**

*From the [‡]Institut für Biochemie und Molekularbiologie, ZBMZ, [§]Fakultät für Biologie, [¶]Institut für Biologie II, Fakultät für Biologie, Funktionelle Proteomik, and [‖]BIOSS Centre for Biological Signaling Studies, Universität Freiburg, 79104 Freiburg, Germany and the [**]Centre de Génétique Moléculaire, CNRS, 91190 Gif-sur-Yvette, France*

**Background:** The TIM23 machinery cooperates with partner protein complexes of the inner mitochondrial membrane to drive preprotein import.
**Results:** The mitochondrial ADP/ATP carrier is efficiently copurified with TIM23 complexes independently of the respiratory chain.
**Conclusion:** The ADP/ATP carrier is an integral part of the TIM23 protein network and supports preprotein import.
**Significance:** This study reveals an unexpected link between mitochondrial protein biogenesis and metabolite transport.

**The majority of mitochondrial proteins are synthesized with amino-terminal signal sequences. The presequence translocase of the inner membrane (TIM23 complex) mediates the import of these preproteins. The essential TIM23 core complex closely cooperates with partner protein complexes like the presequence translocase-associated import motor and the respiratory chain. The inner mitochondrial membrane also contains a large number of metabolite carriers, but their association with preprotein translocases has been controversial. We performed a comprehensive analysis of the TIM23 interactome based on stable isotope labeling with amino acids in cell culture. Subsequent biochemical studies on identified partner proteins showed that the mitochondrial ADP/ATP carrier associates with the membrane-embedded core of the TIM23 complex in a stoichiometric manner, revealing an unexpected connection of mitochondrial protein biogenesis to metabolite transport. Our data indicate that direct TIM23-AAC coupling may support preprotein import into mitochondria when respiratory activity is low.**

Mitochondria are known as structurally and functionally versatile organelles that are the major sites of ATP synthesis in eukaryotic cells under aerobic conditions. They are surrounded by an outer membrane that mediates the communication of mitochondria with other parts of the cell and encompasses the highly folded, protein-rich inner membrane. The enzymatic machineries for ATP production from ADP and inorganic phosphate by oxidative phosphorylation are mainly found in the cristae domains of the inner mitochondrial membrane (1–3), where they associate physically to form different types of supercomplexes (4, 5). Mitochondrial metabolite carrier proteins termed ADP/ATP carriers (AAC)[4] mediate the export of ATP synthesized within mitochondria (6–10). Both ADP/ATP exchange across the inner mitochondrial membrane and import of phosphate into the matrix are crucial for oxidative phosphorylation to proceed (11).

The biogenesis and maintenance of healthy mitochondria is a complicated process because the vast majority of mitochondrial proteins is encoded by nuclear genes and synthesized in the cytosol. Nuclear-encoded mitochondrial proteins are produced as preproteins equipped with specific targeting information that guides them to their final destination. The most frequently found targeting signals are amino-terminal, cleavable presequences that direct preproteins to the inner mitochondrial membrane or the central matrix compartment (12, 13). Presequence-carrying preproteins are imported by the general translocase of the outer membrane (TOM complex) and the presequence translocase of the inner membrane (TIM23 complex) in a membrane potential ($\Delta\psi$)-dependent fashion. The essential, membrane-bound core of the TIM23 complex ($TIM23^{CORE}$) is composed of the Tim17, Tim23, and Tim50 subunits and constitutes the preprotein receptor domain and the protein-conducting channel (14–18). $TIM23^{CORE}$ associates dynamically with different energy-converting partner pro-

* This work was supported by the Deutsche Forschungsgemeinschaft, Sonderforschungsbereich 746; by the Excellence Initiative of the German Federal and State Governments (EXC 294 BIOSS); and by a postdoctoral fellowship of the Peter and Traudl Engelhorn Foundation (to H. R.).
[S] This article contains supplemental Table S1.
[1] Present address: DZD-Paul Langerhans Institut, Universitätsklinikum Carl Gustav Carus an der Technischen Universität Dresden, 01307 Dresden, Germany.
[2] Present address: Department of Neurobiology, Harvard Medical School, Boston, MA 02115.
[3] To whom correspondence should be addressed: Institut für Biochemie und Molekularbiologie, ZBMZ, Universität Freiburg, Stefan-Meier-Str. 17, 79104 Freiburg, Germany. Tel.: 49-761-203-5270; Fax: 49-761-203-5261; E-mail: martin.van.der.laan@biochemie.uni-freiburg.de.

[4] The abbreviations used are: AAC, ADP/ATP carrier; TIM, translocase of the inner membrane; TOM, translocase of outer mitochondrial membrane; PAM, presequence translocase-associated import motor; SILAC, stable isotope labeling with amino acids in cell culture; i-form, intermediate form; $Ni^{2+}$-NTA, nickel-nitrilotriacetic acid; Tricine, *N*-[2-hydroxy-1,1-bis(hydroxymethyl)ethyl]glycine; DHFR, dihydrofolate reductase.

tein complexes at the inner membrane. Via the adaptor proteins Tim21 and Mgr2, $TIM23^{CORE}$ is coupled to respiratory chain supercomplexes composed of the cytochrome $bc_1$ complex (complex III) and cytochrome *c* oxidase (complex IV) (19–26). This TIM23 complex form was termed $TIM23^{SORT}$ because it is sufficient for the solely $\Delta\psi$-driven lateral sorting of preproteins with an additional hydrophobic stop-transfer segment adjacent to the presequence into the inner membrane (27). For the ATP-dependent translocation of preproteins into the aqueous matrix, $TIM23^{CORE}$ cooperates with the presequence translocase-associated import motor (PAM) that is composed of mitochondrial heat shock protein 70 (mtHsp70) and five cochaperones that differentially regulate the import-driving ATPase activity of mtHsp70 and the assembly status of PAM: Tim44, Pam16, Pam17, Pam18, and Mge1 (15–18). The biogenesis of presequence-carrying polytopic inner membrane proteins has been shown to require a close cooperation of the TIM23/PAM machinery with the export translocase Oxa1 (28–30). Therefore, the TIM23 complex acts as an intricate multipurpose molecular machine in which the coupling of distinct partner proteins to $TIM23^{CORE}$ generates functional specificity.

It has been suggested that also AAC proteins may interact with the TIM23 complex, but this association was considered unspecific or mainly indirect via respiratory chain complexes (24, 31, 32). We performed a comprehensive analysis of the $TIM23^{CORE}$ interactome in the yeast *Saccharomyces cerevisiae* on the basis of stable isotope labeling with amino acids in cell culture (SILAC) combined with mass spectrometry and identified the abundant metabolite carrier AAC as a major interaction partner. Surprisingly, we found that purified TIM23 complexes contain AAC and the channel-forming core subunit Tim23 in a 1:1 ratio. Formation of the TIM23-AAC supercomplex is independent of respiratory chain complexes and may facilitate preprotein import primarily under conditions where respiration is compromised.

## EXPERIMENTAL PROCEDURES

*Yeast Strains, Growth Conditions, and Isolation of Mitochondria*—Yeast strains expressing protein A-tagged Tim23 ($Tim23_{ProtA}$) have been described previously (19, 25, 31). $Tim23_{ProtA}$ *rho*− cells were generated by three passages of $Tim23_{ProtA}$ *rho*+ cells onto YPD (1% (w/v) yeast extract, 2% (w/v) bacto peptone, and 2% (w/v) glucose) agar plates containing ethidium bromide. For generation of the mutant strain *tim17-11* (*MATa, ade2–101_ochre, his3-Δ200, leu2-Δ1, ura3–52, trp1-Δ63, lys2–801_amber, tim17::ADE2, [pBG-TIM17-11B]*) (3219), YPH499 wild-type yeast cells were transformed with a pYEp352 plasmid encoding the *TIM17* wild-type allele together with a *URA3* selection marker. In this strain, the chromosomal *TIM17* locus was disrupted by an *ADE2* cassette. Subsequently, a second plasmid encoding the *TIM17-11* allele, which was generated by error-prone PCR, and a *TRP1* selection marker was introduced. The plasmid carrying wild-type *TIM17* was then removed by selection on 5-fluoroorotic acid-containing medium (33). The corresponding wild-type strain (3216) was generated in the same way, except that the remaining plasmid carried a wild-type copy of the *TIM17* gene. Both the *tim17-11* and corresponding wild-type strain were modified to express a protein A-tagged version of Tim23 from the chromosome as described previously (25). For preparation of mitochondria, yeast cells were grown in liquid YPG (1% (w/v) yeast extract, 2% (w/v) bacto peptone, and 3% (v/v) glycerol) or YPGal (1% (w/v) yeast extract, 2% (w/v) bacto peptone, and 2% (w/v) galactose) medium at 30 °C, except for strains carrying the *tim17-11* allele and corresponding wild-types, which were grown in YPG medium at 23 °C. Isolated mitochondria were obtained by differential centrifugation as described previously (34) and suspended in SEM buffer (10 mM MOPS, 1 mM EDTA, and 250 mM sucrose (pH 7.2)) at a total protein concentration of 10 mg/ml. Aliquots were shock-frozen in liquid nitrogen and kept at −80 °C.

*Immunoglobulin G Affinity Chromatography*—Isolated mitochondria were resuspended in digitonin buffer (20 mM Tris-HCl (pH 7.4), 50–60 mM NaCl, 0.25 mM EDTA, 0.7% (w/v) digitonin, 10% (v/v) glycerol, 2 mM PMSF, and 1× EDTA-free protease inhibitor cocktail (Roche)) and incubated for 30 min at 4 °C, shaking head-over-head. After a clarifying spin, the supernatant containing solubilized membrane protein complexes was incubated with human IgG (Sigma-Aldrich) coupled to cyanogen bromide-activated Sepharose beads (GE Healthcare). Samples were incubated for 2–3 h at 4 °C, shaking head-over-head. Protein-loaded beads were collected by centrifugation and washed six to ten times with eight bed volumes of wash buffer (20 mM Tris-HCl (pH 7.4), 60 mM NaCl, 0.25–0.5 mM EDTA, 0.3% (w/v) digitonin, 10% (v/v) glycerol, and 2 mM PMSF). Elution of bound protein complexes was achieved by cleavage with tobacco etch virus protease (Invitrogen) for 15 h at 4 °C under strong shaking.

*Preprotein Import into Mitochondria*—$^{35}$S-labeled preproteins were synthesized with the $T_NT$ coupled transcription/translation system (Promega, Madison, WI) and incubated with isolated mitochondria in import buffer (10 mM MOPS (pH 7.2), 250 mM sucrose, 80 mM KCl, 5 mM methionine, 5 mM $MgCl_2$, 2 mM $KH_2PO_4$, and 4 mM ATP) at 25 °C. Import reactions were analyzed by SDS-PAGE and autoradiography. Radiolabeled protein bands were quantified using Fiji software (35).

The inward-directed force generated by the import motor PAM was analyzed using the model preprotein $b_2$(220)-DHFR (19). The preprotein was preincubated for 5 min with 5 μM methotrexate in import buffer supplemented with 3% (w/v) BSA, 4 mM NADH, 10 mM creatine phosphate, and 0.2 mg/ml creatine kinase. Mitochondria were added, and reaction mixtures were incubated for 20 min at 25 °C. Thereafter, $\Delta\psi$ was uncoupled by the addition of 10 μM valinomycin. Reactions were further incubated for different time periods, stopped by transfer to ice, and treated with 50 μg/ml proteinase K where indicated. To assess the import-driving force, the proteinase K-resistant intermediate (i) form of $b_2$(220)-DHFR was quantified. Values were normalized to the amount of i-form generated during the first incubation in the presence of $\Delta\psi$ without proteinase K treatment.

To gradually dissipate $\Delta\psi$, mitochondria were diluted into import buffer supplemented with 0.7% (w/v) BSA, 4 mM NADH, 10 mM creatine phosphate, 0.2 mg/ml creatine kinase, 20 μM oligomycin, and 0–40 μM carbonyl cyanide *m*-chloro-

phenylhydrazone (21, 25). To analyze import reactions energized by ADP/ATP exchange, 10 $\mu$M antimycin A, 20 $\mu$M oligomycin, 10 mM creatine phosphate, 0.2 mg/ml creatine kinase, and 20 $\mu$M carboxyatractyloside were added to mitochondria in import buffer containing 1.5% (w/v) BSA as indicated.

*Quantitative Analysis of Mitochondrial Protein Complexes*—TIM23 complexes were purified from isolated mitochondria via protein A-tagged Tim23. The RTS 100 wheat germ CECF kit (5 Prime, Hilden, Germany) was used for cell-free protein synthesis according to the instructions of the supplier. Proteins were produced with C-terminal hexahistidine tags for subsequent purification. Wheat germ lysates containing the proteins of interest were diluted 12.5× in buffer A (50 mM sodium phosphate (pH 8.0), 300 mM NaCl, 0.5% (w/v) SDS, 2 mM PMSF, and 1× EDTA-free protease inhibitor cocktail (Roche)) supplemented with 5 mM imidazole and incubated with pre-equilibrated PerfectPro $Ni^{2+}$-NTA agarose beads (5 Prime) for 1 h at room temperature. Protein-loaded $Ni^{2+}$-NTA beads were washed extensively with buffer A containing 10 mM imidazole, and bound proteins were eluted with buffer B (50 mM sodium phosphate (pH 7.0), 300 mM NaCl, 300 mM imidazole, 0.5% (w/v) SDS, 2 mM PMSF, and 1× EDTA-free protease inhibitor cocktail (Roche)). Different volumes of the elution fractions were analyzed by SDS-PAGE and colloidal Coomassie staining together with multiple defined amounts of a protein standard (low molecular weight calibration kit (GE Healthcare)). Stained protein bands were quantified using MultiGauge software (Fujifilm, Tokyo, Japan). The concentrations of purified proteins in the $Ni^{2+}$-NTA elution fractions were calculated from the given protein amounts in the protein standard bands of comparable molecular weight. Subsequently, different amounts of the elution fractions of TIM23 complex isolations from mitochondria and the respective *in vitro*-synthesized purified proteins were analyzed by 6–16.5% Tris-Tricine SDS-PAGE and Western blotting using antisera against Tim23, AAC, Yhm2, or Pam18. The amounts of the different proteins recovered in the elution fractions of TIM23 complex isolations were calculated and normalized to the amount of the bait protein Tim23. The total amount of Yhm2 in isolated mitochondria was calculated in a similar way using purified Yhm2 as a standard (25).

*SILAC, MS, and Data Analysis*—Wild-type yeast cells were grown in the presence of [$^{13}C_6$]lysine and [$^{13}C_6$]arginine, whereas cells expressing protein A-tagged Tim23 ($Tim23_{ProtA}$) were grown in the presence of standard $^{12}C$-containing amino acids (25). Mitochondria were isolated from both strains and mixed in equal amounts (total protein content). Subsequently, mitochondria were lysed in digitonin buffer, and detergent extracts were subjected to IgG affinity chromatography. Purified TIM23 complexes were acetone-precipitated, followed by proteolytic digestion with trypsin. Nano-HPLC/ESI-MS/MS analyses of the resulting peptide mixtures of three independent replicates were performed using an UltiMate™ 3000 HPLC system (Dionex LC Packings/Thermo Fisher Scientific, Idstein, Germany) coupled directly to an LTQ-Orbitrap XL instrument (Thermo Fisher Scientific). Peptides were first loaded onto a C18 micro-precolumn (0.3 mm inner diameter × 5 mm; PepMap, Dionex LC Packings/Thermo Fisher Scientific), preconcentrated and washed in 0.1% (v/v) trifluoroacetic acid (flow rate, 30 $\mu$l/min), and then separated on a C18 reverse-phase nano-LC column (75 $\mu$m inner diameter × 150 mm; PepMap, Dionex LC Packings/Thermo Fisher Scientific). For peptide elution, a 150-min linear gradient with increasing concentrations of acetonitrile (4–34% (v/v)) in 0.1% (v/v) formic acid was applied at a flow rate of 300 nl/min. The LTQ-Orbitrap was equipped with a nano-ESI source (Thermo Fisher Scientific) and was operated in a data-dependent mode acquiring high-resolution MS precursor scans in the Orbitrap (*m/z* 300–1500; resolution, 60,000 at *m/z* 400; automatic gain control, $5 \times 10^5$; maximum fill time, 500 ms). Concomitantly, up to six of the most intense multiply charged ions were further fragmented by low-energy, collision-induced dissociation in the linear ion trap (automatic gain control, $1 \times 10^4$; maximum fill time, 100 ms). Collision-induced dissociation was performed at a normalized collision energy of 35%, applying a Mathieu stability parameter q value of 0.25 and an activation time of 30 ms. The dynamic exclusion time was set to 45 s. Mass spectrometric raw data were processed using MaxQuant (version 1.0.13.13) in combination with the search engine Mascot (version 2.2). For peptide and protein identification, MS/MS data were searched against a decoy database derived from the *Saccharomyces* Genome Database using the following parameters: mass tolerances for precursor and fragment ions, 7 ppm and 0.5 Da, respectively; methionine oxidation as variable modification; proteolytic enzyme, trypsin; maximum of missed cleavages, 2; and at least one unique peptide with a minimum of six amino acids. A false discovery rate of <1% was applied on both the peptide and protein levels. Relative protein quantification was performed on the basis of differentially [$^{12}C_6$]/[$^{13}C_6$]arginine- and [$^{12}C_6$]/[$^{13}C_6$]lysine-labeled unique peptides and a minimum ratio count of one. Low-scoring variants of identified peptides were not considered for quantification. For data visualization, the mean of $\log_{10}$-transformed SILAC (light/heavy) ratios were calculated and plotted against the *p* value ($-\log_{10}$) determined for each protein using a one-sided Student's *t* test.

## RESULTS

*Interactome of the TIM23 Core Complex*—To obtain a compendium of TIM23-interacting proteins, we differentially labeled yeast cells that expressed either an unmodified (wild-type) or protein A-tagged version of the presequence translocase core component Tim23 from the chromosome. Isolated mitochondria of both strains were mixed and solubilized under mild conditions with the non-ionic detergent digitonin. The resulting detergent extracts were subjected to IgG affinity chromatography. Mass spectrometric analysis of the elution fractions was performed, and light-over-heavy peptide ratios were assigned to the identified proteins. In this way, we obtained the first comprehensive view of the interactome of the TIM23 complex (Fig. 1*A*; for a complete list of identified proteins, see supplemental Table S1). Among the most enriched proteins were the known core components Tim17, Tim23, and Tim50, the $TIM23^{SORT}$-specific subunits Tim21 and Mgr2, components of the import motor PAM, and subunits of respiratory chain supercomplexes, indicating that both major forms of the TIM23 complex were recovered. The group of further identi-

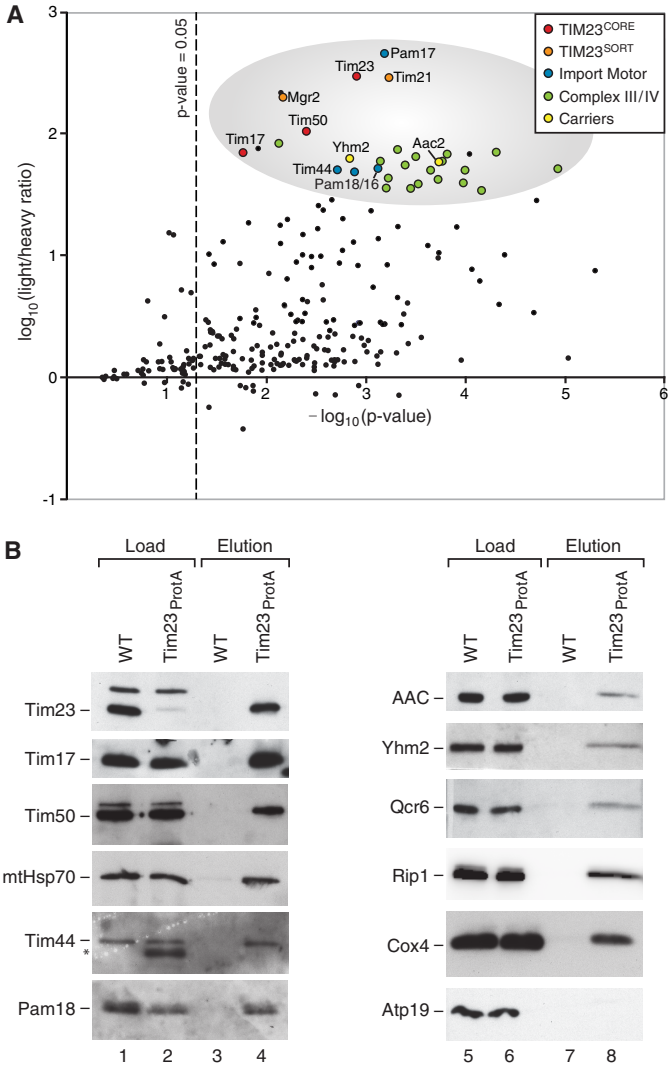


FIGURE 1. **Interactome of the TIM23 complex.** *A*, yeast cells were grown in [$^{13}C_6$]lysine- and [$^{13}C_6$]arginine-containing (wild-type) or standard $^{12}C$ amino acid-containing ($Tim23_{ProtA}$) medium. Mitochondria were isolated, mixed, and lysed with digitonin. Detergent extracts were used for IgG affinity chromatography. Elution fractions were analyzed by mass spectrometry as described under "Experimental Procedures". The mean $\log_{10}$ light-over-heavy ratios of three independent experiments were calculated and plotted against the corresponding *p* values ($-\log_{10}$). Proteins with a light-over-heavy ratio of >30 are highlighted by a *gray oval*. *Red*, components of $TIM23^{CORE}$; *orange*, subunits specifically present in the $TIM23^{SORT}$ form; *blue*, PAM; *green*, respiratory chain complexes III (cytochrome $bc_1$) and IV (cytochrome *c* oxidase); *yellow*, mitochondrial carrier family proteins; *black*, further identified proteins. (The complete list of identified and quantified proteins can be found in supplemental Table S1.) *B*, affinity chromatography experiments performed with unlabeled WT and $Tim23_{ProtA}$ mitochondria. Samples were analyzed by SDS-PAGE and immunoblotting with the indicated antisera. Elution, 100%; load, TIM/PAM proteins, 17%; respiratory chain subunits and metabolite carriers, 2%. *mtHsp70*, mitochondrial heat shock protein 70; *asterisk*, signal derived from $Tim23_{ProtA}$.

fied proteins enriched with $Tim23_{ProtA}$ contained subunits of known partner protein complexes like the TOM complex (Tom40, Tom22, and Tom20) and the oxidase assembly (OXA) machinery (Oxa1) that transiently cooperate with TIM23 (15–18, 29, 30) as well as several respiratory chain assembly factors that may link import and sorting of respiratory chain proteins to their incorporation into mature complexes. A dual role as TIM23-associated component and complex IV assembly factor has been demonstrated for human TIM21 (36). Among the most enriched proteins in our TIM23 interactome dataset was a so far uncharacterized protein termed Aim19. Deletion of the *AIM19* gene leads to a mild respiratory growth defect (37), and a proteomic analysis identified Aim19 as a potential interaction partner of respiratory chain supercomplexes (38), which may explain its strong enrichment with tagged Tim23. Moreover, subunits of the mitochondrial contact site and cristae organizing system (MICOS complex) (39) that is required for the formation of crista junctions were found to be enriched with Tim23 (Mic10, Mic12, Mic27, and Mic60), albeit with lower efficiency. A recent study has shown that active preprotein import sites containing TOM and TIM23 complexes tethered by a preprotein in transit form distinct clusters that are preferentially located in the vicinity of crista junctions (40), pointing to a possible link between the mitochondrial contact site and cristae organizing system and the preprotein import machinery.

Interestingly, we found several mitochondrial metabolite carriers in the TIM23 interactome. Two members of this abundant protein family, the major ADP/ATP carrier isoform Aac2 and the citrate/oxoglutarate carrier Yhm2 (41), were among the most enriched proteins, together with PAM and respiratory chain subunits (Fig. 1*A*). These proteins were also detected in our recent proteomic analysis of only the $TIM23^{SORT}$ form that led to the identification of the Mgr2 subunit (25). Because metabolite carrier proteins are imported via the carrier translocase of the inner membrane (TIM22 complex) (42), a copurification of AAC and Yhm2 as client proteins seems highly unlikely. Western blot analysis of label-free TIM23 complex purifications via $Tim23_{ProtA}$ confirmed the efficient coisolation of the $TIM23^{CORE}$ and PAM components as well as respiratory chain subunits (Qcr6 and Rip1 of complex III and Cox4 of complex IV) with Tim23 under our experimental conditions (Fig. 1*B*). Both AAC and Yhm2 were similarly detected in the elution fraction, whereas subunits of other highly abundant protein complexes of the inner mitochondrial membrane, like Atp19 of the $F_1F_o$-ATP synthase, were not recovered.

*AAC Associates with TIM23 Complexes in a Stoichiometric Manner*—Our previous analysis of total mitochondrial protein levels had shown that AAC is ~18 times more abundant than Tim23 (25). We determined the total amount of Yhm2 in isolated yeast mitochondria using the same biochemical approach. Yhm2 was present at ~16 pmol/mg of mitochondrial protein, which is virtually identical to the amount of Tim23 (25). Therefore, a comparison of the Western blot signals obtained for TIM23 core subunits and Yhm2 in the load and elution fractions of $Tim23_{ProtA}$ isolations (Fig. 1*B*) suggests that Yhm2 is associated with TIM23 in a substoichiometric manner. However, in this type of analysis, the large difference in the total amounts of AAC and Tim23 made it difficult to estimate how much AAC is bound to TIM23 complexes. Divergent views have been reported before on the significance and specificity of a putative interaction between AAC and TIM23. AAC recovered with protein A-tagged Tim23 in an earlier label-free study was considered contamination (31). Another study, in which a hexahistidine tag on the Aac2 protein was used, came to the conclusion that TIM23 mainly interacts with large supercomplexes composed of respiratory chain complexes and AAC (24).

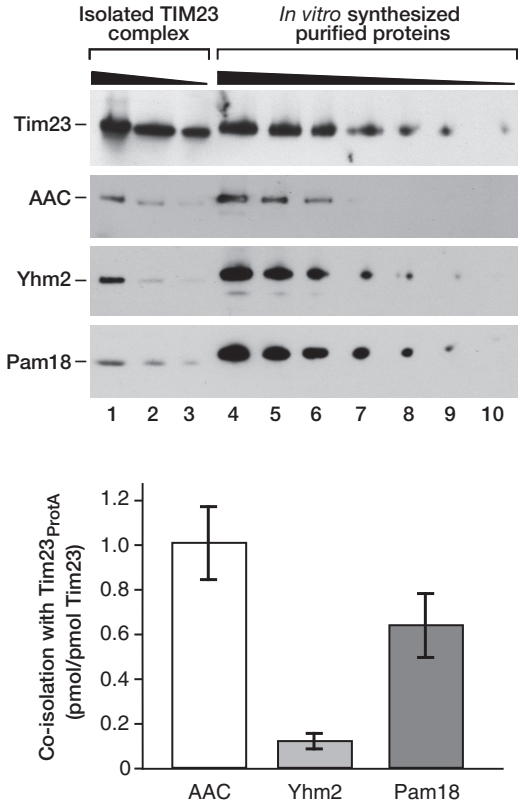


FIGURE 2. **AAC associates with TIM23 complexes in a stoichiometric manner.** TIM23 complexes were purified from digitonin-solubilized mitochondria via protein A-tagged Tim23. The mitochondrial proteins Tim23, AAC (major isoform Aac2), Yhm2, and Pam18 were synthesized in a cell-free system and purified. The concentrations of purified proteins were determined as described under "Experimental Procedures." Different amounts of isolated TIM23 complexes (*lanes 1–3*) and *in vitro*-synthesized, purified proteins (*lanes 4–10*) were analyzed by Tris-Tricine SDS-PAGE and immunoblotting with the indicated antisera. Because of the presence of a hexahistidine tag for purification, the *in vitro*-synthesized proteins show a slightly slower migration in the gel than their mitochondrial counterparts. *Bottom panel*, the molar amounts of AAC, Yhm2, and Pam18 recovered in the elution fractions of TIM23 complex isolations were calculated and normalized to the amount of the tagged bait protein Tim23. Data are mean ± S.E. ($n = 3$).

However, a proteomic analysis of the AAC interactome on the basis of affinity purification experiments with tagged Aac2 identified respiratory chain complexes, but not TIM23 components, as candidate partner proteins (43). Notably, it has also been reported that affinity tags on Aac2 might considerably influence its interaction with partner proteins (32).

Therefore, we decided to directly determine the amount of AAC associated with TIM23 complexes in the presence of unmodified AAC by a quantitative Western blotting approach that we established earlier to determine the amount of Mgr2 associated with $TIM23^{SORT}$ (25). In brief, mitochondrial proteins were synthesized in a cell-free system and purified. Different defined concentrations of the purified proteins were then compared directly with the amounts of the respective proteins recovered in the elution fractions of TIM23 complex isolations via $Tim23_{ProtA}$. The surprising result of these experiments was that AAC is coisolated with Tim23 in a molar ratio of ~1:1 (Fig. 2). In contrast to AAC, Yhm2 was ten times less abundant in the elution fractions of TIM23 complex isolations than the tagged bait protein Tim23 (Fig. 2). It should be noted here that the light-over-heavy SILAC ratios reflect the specificity of coisolation for a given protein (relative enrichment with the tagged bait over the untagged wild-type control sample) but not the absolute protein amount in the elution fractions. Our quantitative Western blot analysis revealed that, despite similar SILAC ratios, the absolute protein amounts of AAC and Yhm2 and their molar stoichiometry to the bait protein Tim23 in the elution fractions differ by one order of magnitude. Moreover, we quantified the amount of the import motor component Pam18 isolated with tagged Tim23. It is assumed that Pam18 and Tim23 are present in equimolar amounts in the coupled TIM23/PAM machinery (17) but that not all $TIM23^{CORE}$ complexes in mitochondria are associated with PAM (18). In agreement with these models, our quantitative analysis of TIM23 complex isolations revealed that a substoichiometric amount of Pam18 is coisolated with tagged Tim23 (~0.6 pmol Pam18/1 pmol of Tim23 in the elution fraction) (Fig. 2).

*AAC Binds to TIM23 Independently of the Respiratory Chain*—Our finding that AAC is coisolated with tagged Tim23 in a 1:1 ratio is difficult to reconcile with the hypothesis that AAC mainly associates with TIM23 complexes indirectly via respiratory chain supercomplexes (24) because the latter have been shown before to interact selectively with $TIM23^{SORT}$ complexes (21, 22). To directly assess the mutual dependence of respiratory chain and AAC interactions with TIM23, we generated a yeast strain that expressed protein A-tagged Tim23 in the presence of unmodified AAC but lacked mitochondrial DNA and, therefore, assembled respiratory chain complexes ($Tim23_{ProtA}$ *rho*−). We isolated mitochondria from $Tim23_{ProtA}$ *rho*− and, for comparison, $Tim23_{ProtA}$ *rho*+ cells, both grown in fermentable medium (YPGal), solubilized them under mild conditions as described above, and performed affinity purification experiments. For the $TIM23^{CORE}$ subunit Tim17, both the steady state protein levels in the detergent extracts of mitochondria (Fig. 3*A*, *lanes 1* and *2*) and the coisolation efficiency with tagged Tim23 (Fig. 3*A*, *lanes 3* and *4*) were similar in *rho*+ and *rho*− mitochondria. Therefore, the loss of mitochondrial DNA did not considerably affect the amount and assembly state of $TIM23^{CORE}$. The protein levels of nuclear-encoded respiratory chain complex subunits, like Cox4, were strongly reduced in *rho*− mitochondria as expected (Fig. 3*A*, *lanes 1* and *2*). Unassembled Cox4 was not detectable in the elution fractions of $Tim23_{ProtA}$ *rho*− isolations, indicating that fully assembled respiratory chain complexes, but not individual subunits, associate with TIM23 complexes (Fig. 3*A*, *lanes 3* and *4*) (21, 27). For AAC, we obtained a differential result. Although the total protein levels in detergent extracts of mitochondria were reduced strongly in *rho*− compared with *rho*+ mitochondria (Fig. 3, *A*, *lanes 1 and 2*, and *B*), the amount of AAC coisolated with tagged Tim23 was only reduced moderately (Fig. 3, *A*, *lanes 3* and *4*, and *B*). Therefore, AAC associates efficiently with TIM23 complexes in the absence of assembled respiratory chain complexes. Because the coisolation of AAC with tagged Tim23 does not depend on respiratory chain complexes, we conclude that the major fraction of AAC recovered with the purified TIM23 machinery is directly associated with $TIM23^{CORE}$ complexes.

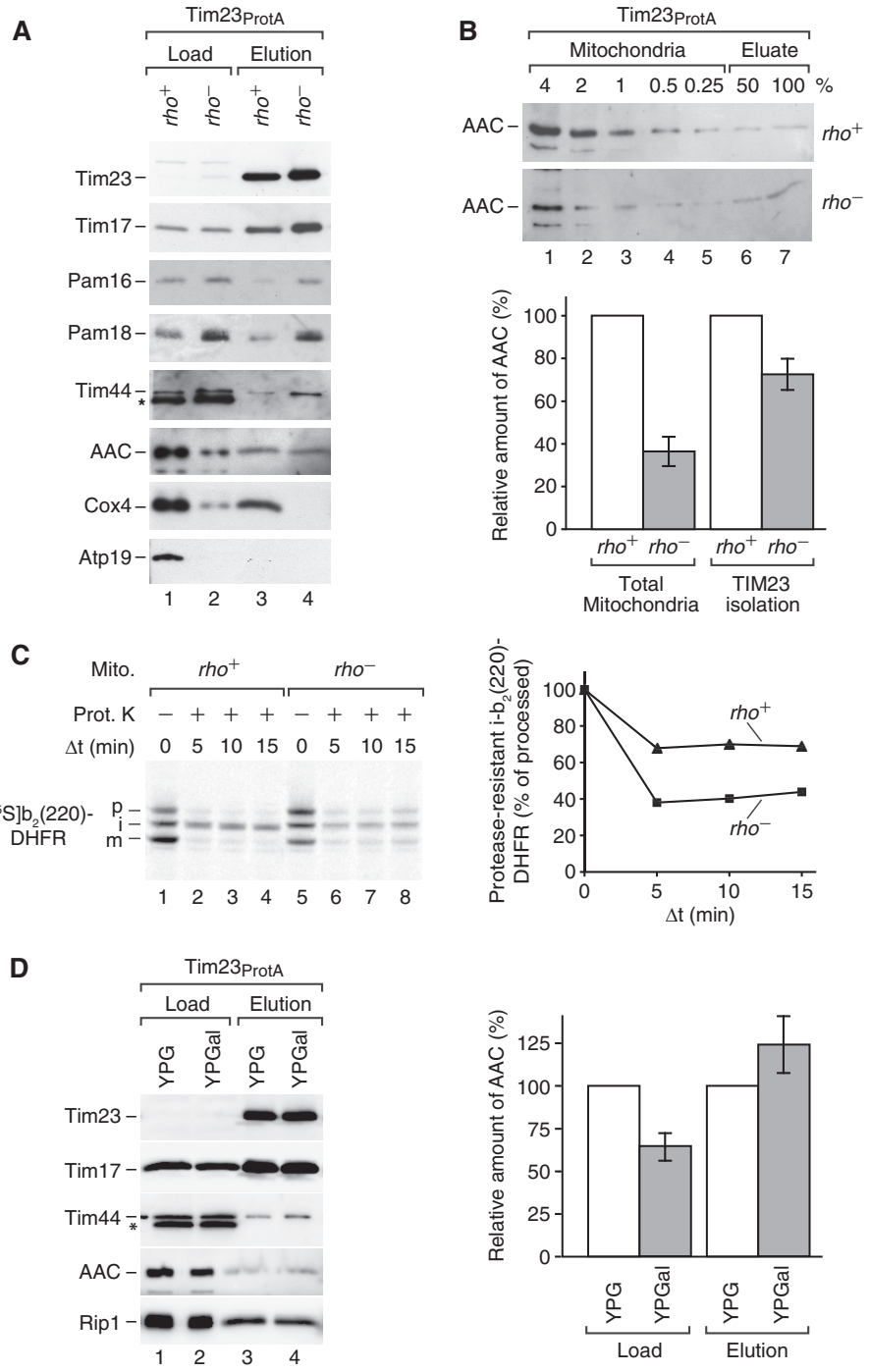


FIGURE 3. **AAC efficiently binds to TIM23 in the absence of respiratory chain complexes.** *A*, TIM23 complexes were purified from *rho*+ and *rho*− mitochondria via protein A-tagged Tim23 and subsequently analyzed by SDS-PAGE and immunoblotting. Elution, 100%; load, TIM/PAM subunits, 17%; respiratory chain subunits and AAC, 2%. *Asterisk*, signal derived from $Tim23_{ProtA}$. *B*, comparison of the relative amounts of AAC in Western blot titrations of solubilized $Tim23_{ProtA}$ *rho*+ and $Tim23_{ProtA}$ *rho*− mitochondria (*lanes 1–5*) and in the corresponding elution fractions of TIM23 complex isolations (*lanes 6* and *7*). *Bottom* panel, Western blot signals were quantified using ImageQuant software. Data are mean ± range ($n = 2$). The amounts detected in the *rho*+ samples were set to 100%. *C*, import-driving activity generated by the import motor PAM was analyzed in *rho*+ and *rho*− mitochondria (*Mito*) as described under "Experimental Procedures." $[^{35}S]b_2(220)$-DHFR was incubated with isolated mitochondria in the presence of methotrexate. After a second incubation (Δt) in the absence of $\Delta\psi$, samples were treated with proteinase K (*Prot. K*) as indicated and subjected to SDS-PAGE. Radiolabeled protein bands were visualized by digital autoradiography. *Right panel*, the amount of the protease-resistant intermediate form (*i*) of $b_2(220)$-DHFR in *lanes 2–4* and *lanes 6–8* was quantified using Fiji software and normalized to the amount of the i-form generated at $\Delta t = 0$ in the respective import reaction. The mature (m-)form of $b_2(220)$-DHFR is generated by a second processing step in the intermembrane space releasing the protein from the inner mitochondrial membrane. *p*, preprotein. *D*, $Tim23_{ProtA}$ mitochondria isolated from cells grown in fermentable (YPGal) or non-fermentable (YPG) media were solubilized, subjected to affinity chromatography, and analyzed as in *A*. Western blot signals obtained for AAC in the load (*lanes 1* and *2*), and elution (*lanes 3* and *4*) fractions were quantified using Fiji software (*right panel*). AAC signals in the elution fractions were normalized to the amounts of the eluted bait protein Tim23. The AAC amounts detected in YPG samples were set to 100%. Data are mean ± S.E. ($n = 3$).

Furthermore, we observed an enhanced association of import motor components, like Pam16, Pam18, and Tim44, with $TIM23^{CORE}$ (Fig. 3*A*, *lanes 3* and *4*) in *rho*− mitochondria, suggesting that the equilibrium of the different TIM23 forms (19, 27) was shifted toward the PAM-bound form. We asked how this enhanced PAM coupling to TIM23 affects the inward-directed force generated by the import motor on a preprotein at the expense of ATP hydrolysis (17, 19). To address this question, we used the model preprotein $b_2$(220)-DHFR, which consists of the N-terminal domain of the nuclear-encoded mitochondrial protein cytochrome $b_2$ fused to DHFR (19, 44). In the presence of methotrexate, the folded state of the DHFR moiety is stabilized so that the cytochrome $b_2$ portion of the preprotein is imported into mitochondria, whereas the folded DHFR moiety remains on the mitochondrial surface, leading to the formation of a two-membrane-spanning translocation intermediate. The matrix-targeting signal of $b_2$(220)-DHFR is removed by the mitochondrial processing peptidase, leading to the formation of an i-form. Upon accumulation of $b_2$(220)-DHFR in import sites, $\Delta\psi$ was dissipated to eliminate its contribution to the inward-directed force on the preprotein (45). After different time periods, samples of the import reaction were treated with proteinase K. In *rho*+ mitochondria the activity of the ATP-driven import motor efficiently "pulled" the folded DHFR moiety of the preprotein against the outer mitochondrial membrane so that a substantial fraction of the accumulated i-form remained protected against digestion with proteinase K (Fig. 3*C*, *lanes 2–4*) (19). In *rho*− mitochondria, the amounts of the proteinase K-resistant i-form were considerably lower compared with *rho*+ mitochondria (Fig. 3*C*, *lanes 6–8*; *right panel*, quantification). Therefore, despite the enhanced coupling of PAM subunits to TIM23 in *rho*− mitochondria, the import-driving activity of the motor was reduced. These data suggest that ATP levels in the mitochondrial matrix are limiting for PAM activity in *rho*− mitochondria that do not synthesize ATP by oxidative phosphorylation.

When *rho*+ yeast cells are grown in a fermentable medium like YPGal, mitochondrial ATP synthesis rates are lower than in cells grown in respiratory medium such as YPG. Cellular ATP is mainly synthesized by substrate-level phosphorylation in the cytosol under fermentative growth conditions (46). In mitochondria isolated from $Tim23_{ProtA}$ *rho*+ cells grown in YPGal, we detected reduced overall levels of AAC compared with mitochondria from cells grown in YPG (Fig. 3*D*, *lanes 1* and *2*; *right panel*, quantification). However, the amount of AAC coisolated with tagged Tim23 was similar regardless of using YPGal or YPG for growth of yeast cells (Fig. 3*D*, *lanes 3* and *4*). Therefore, despite the lower overall levels of AAC in cells that import ATP from the cytosol into mitochondria (*rho*− cells, fermentative growth), the TIM23-bound AAC pool is largely retained.

*Coupling of AAC to TIM23 Supports Mitochondrial Protein Import When Respiration Is Compromised*—It has been shown that the transport activity of AAC is not required for preprotein import via TIM23 into actively respiring mitochondria (47, 48). However, when the respiratory activity of mitochondria is very low or absent, like in *rho*− mitochondria, AAC activity is not only important to maintain sufficient matrix ATP levels. In addition, the electrogenic import of ATP (four negative charges) from the cytosol into the mitochondrial matrix in exchange for ADP (three negative charges) generates a $\Delta\psi$ of physiological polarity (*i.e.* negative on the matrix side) (11). It seemed possible that local coupling of TIM23 complexes to AAC as a $\Delta\psi$-generating device may support $\Delta\psi$-dependent preprotein import under such conditions. We aimed to establish an experimental setup to test this idea using the model preprotein Su9-DHFR, which contains the N-terminal mitochondrial targeting sequence of *Neurospora crassa* ATP synthase subunit 9 and the passenger protein DHFR (49). When $\Delta\psi$ generation via the respiratory chain and reverse action of $F_1F_o$-ATP synthase was inhibited by the addition of antimycin A and oligomycin, import of Su9-DHFR was largely blocked (Fig. 4*A*, *lane 1*). Import activity was strongly increased when an ATP-regenerating system (creatine phosphate and creatine kinase) was added to the reaction buffer (Fig. 4*A*, *lane 2*). Import of Su9-DHFR driven by high ATP levels in the presence of antimycin A and oligomycin was blocked when the AAC inhibitor carboxyatractyloside was added (Fig. 4*A*, *lane 3*), demonstrating that the observed import activity depended on AAC-mediated nucleotide exchange. We then used this experimental setup to screen several mutant mitochondria available in our laboratories for specific import defects under such conditions. The mutant yeast strain *tim17-11* (see "Experimental Procedures") was selected initially on the basis of its temperature-sensitive growth phenotype. Mitochondria isolated from *tim17-11* cells grown at permissive temperature imported Su9-DHFR with comparable efficiency as wild-type mitochondria in the absence of inhibitors, demonstrating that the TIM23/PAM machinery was not compromised (Fig. 4*B*). (No considerable differences were observed in the steady-state levels of all mitochondrial proteins tested, including TIM23 and PAM subunits as well as AAC in *tim17-11* and wild-type mitochondria (data not shown).) However, AAC-dependent import of Su9-DHFR in the presence of antimycin A, oligomycin, and an ATP-regenerating system was reduced significantly in *tim17-11* mitochondria (Fig. 4*C*). This import defect was not caused by a reduced $\Delta\psi$ or an increased overall sensitivity of the TIM23 complex toward low $\Delta\psi$ because the response of Su9-DHFR import efficiency to a gradual uncoupling of $\Delta\psi$ (independent of its source) using carbonyl cyanide *m*-chlorophenylhydrazone (21, 25) was indistinguishable in WT and *tim17-11* mitochondria (Fig. 4*D*). Assessment of the import-driving activity of PAM exerted on $b_2$(220)-DHFR accumulated in import sites demonstrated that the import motor is fully active in *tim17-11* mutant mitochondria (Fig. 4*E*). We then introduced a protein A tag on Tim23 in *tim17-11* and the corresponding wild-type strain. Cells were grown at a permissive temperature, and mitochondria were isolated and solubilized in digitonin buffer. Detergent extracts were used to purify TIM23 complexes by affinity chromatography. Coisolation of AAC with $TIM23^{CORE}$ complexes was reduced considerably in *tim17-11* mutant mitochondria, whereas the amounts of the essential import motor subunit Pam18 in the elution fractions of wild-type and *tim17-11* mitochondria were identical (Fig. 4*F*). Taken together, these data suggest that the selective defect in AAC-dependent preprotein import observed in *tim17-11* mutant mitochondria is mainly caused by an impaired association of TIM23 and AAC.

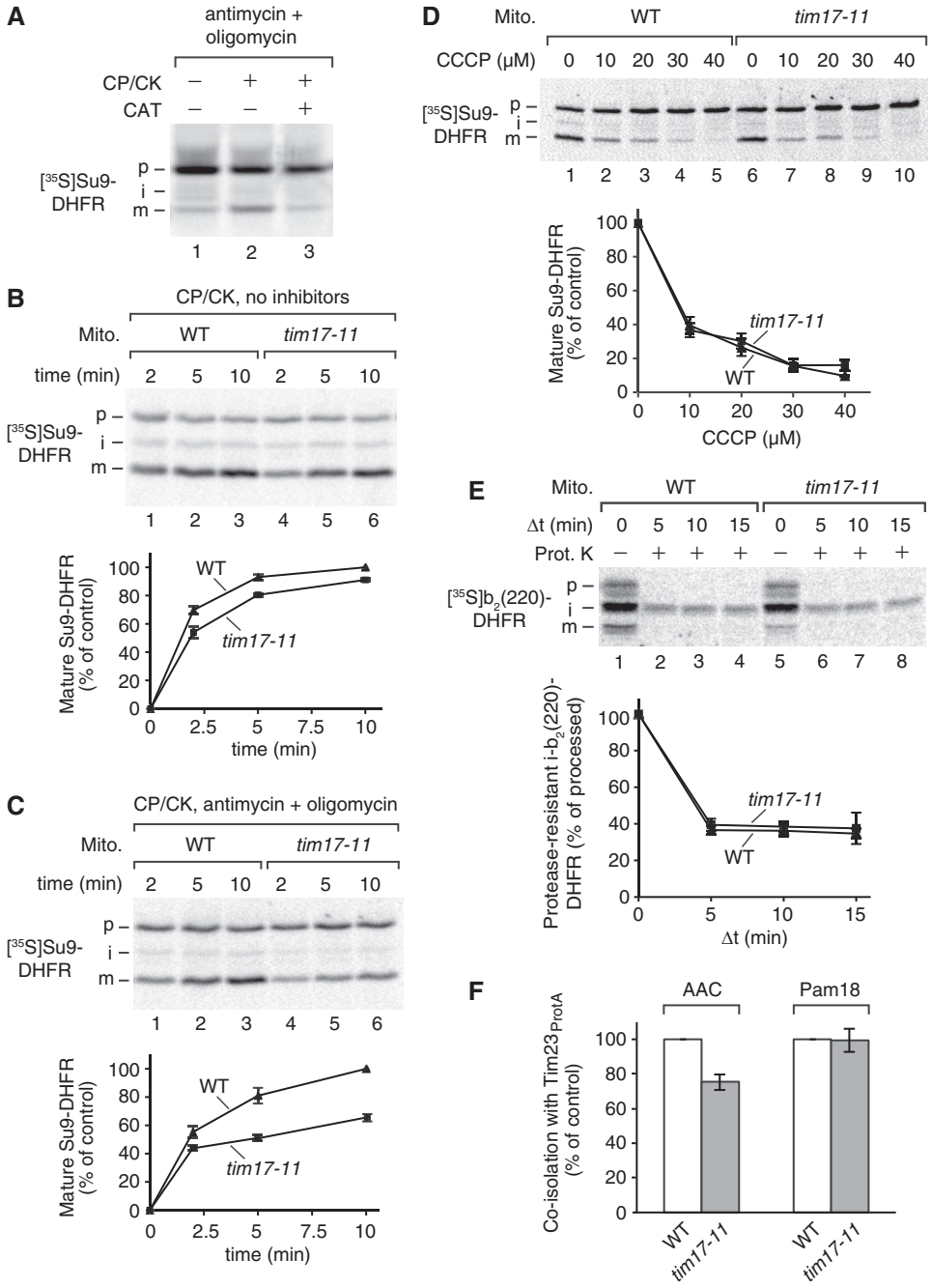


FIGURE 4. **TIM23-AAC coupling supports mitochondrial preprotein import when respiration is compromised.** *A*, $^{35}$S-labeled Su9-DHFR was imported into isolated wild-type (*WT*) mitochondria in the presence of antimycin A and oligomycin. Creatine phosphate (*CP*), creatine kinase (*CK*), and carboxyatractyloside (*CAT*) were added as indicated. Samples were analyzed by SDS-PAGE and autoradiography. *p*, preprotein; *i*, intermediate form; *m*, mature form. *B*, radiolabeled Su9-DHFR was imported into WT and *tim17-11* mutant mitochondria (*Mito*) in the presence of creatine phosphate and creatine kinase. *Bottom panel*, the amount of mature Su9-DHFR was quantified. Import into WT mitochondria after 10 min was set to 100%. Data are mean ± S.E. ($n = 4$). *C*, import reactions were carried out in the presence of creatine phosphate, creatine kinase, antimycin A, and oligomycin and analyzed as in *B*. *D*, $^{35}$S-labeled Su9-DHFR was imported into WT and *tim17-11* mitochondria for 10 min in the presence of oligomycin and the indicated amounts of carbonyl cyanide *m*-chlorophenylhydrazone (*CCCP*). Mature Su9-DHFR signals were quantified. The values obtained in the absence of carbonyl cyanide *m*-chlorophenylhydrazone were set to 100% for WT and *tim17-11* mitochondria. Data are mean ± S.E. ($n = 3$). *E*, the import-driving force generated by the import motor PAM in wild-type and *tim17-11* mitochondria was analyzed and quantified as in Fig. 3*C*. *F*, WT and *tim17-11* mitochondria containing protein A-tagged Tim23 were solubilized with digitonin. Detergent extracts were used for affinity purification of TIM23 complexes. Load and elution fractions were subjected to SDS-PAGE und immunoblotting. Signals were quantified using Fiji software. The amounts of AAC and Pam18 coisolated with tagged Tim23 were normalized to the amounts of the core TIM23 subunit Tim17 detected in the elution fractions. Data are mean ± S.E. (AAC, $n = 5$; Pam18, $n = 4$).

## DISCUSSION

Different views have been reported on the relationship between the ADP/ATP carrier and the protein import machinery of the mitochondrial inner membrane. Our detailed quantitative proteomic and biochemical analyses revealed that isolated TIM23 complexes contain AAC in a ~1:1 ratio compared with the central Tim23 subunit. This is the first demonstration of a stoichiometric association between a metabolite carrier

and a mitochondrial protein translocase. The TIM23-bound pool of AAC, however, only represents a minor fraction of the total amount of the protein in mitochondria because AAC is present in vast excess over $TIM23^{CORE}$ complexes. This may explain why, in earlier studies, the amount of TIM23-bound AAC was underestimated or even appeared below the detection level of the antibodies used. We found that the efficient association of AAC with TIM23 is mostly retained, even when total AAC levels in mitochondria are strongly reduced. This finding underscores the specificity of the TIM23-AAC interaction. The observed decrease of total AAC levels in mitochondria from cells grown under fermentative conditions is in agreement with results of a recent study on the regulation of mitochondrial protein import by reversible phosphorylation. Under fermentative growth conditions, the TOM complex receptor Tom70 becomes phosphorylated by protein kinase A, leading to an inhibition of receptor activity and decreased import of mitochondrial metabolite carriers like AAC (50).

Dienhart and Stuart (24) suggested that the TIM23 machinery mainly associates with a large supercomplex of respiratory chain and AAC. They considered unlikely that AAC is an integral part of the $TIM23^{CORE}$ population because the mobility of TIM23 complexes did not change in the absence of the major AAC isoform Aac2 upon separation of solubilized mitochondrial protein complexes by blue native electrophoresis. Our data, however, show that the association of AAC with TIM23 does not depend on the presence of respiratory chain complexes. We speculate that AAC dissociates from $TIM23^{CORE}$ complexes in wild-type mitochondria during blue native electrophoresis. A similar behavior has been reported for the essential $TIM23^{CORE}$ subunit Tim50 (51). This might explain why the migration of $TIM23^{CORE}$ complexes, as detected in native gels, appeared unaltered when *aac2*Δ mutant mitochondria were analyzed (24).

Our finding that AAC directly associates with TIM23 complexes in a stoichiometric manner amends the current view of preprotein import into mitochondria and highlights the striking potential of SILAC-/MS-based analysis of membrane protein complexes to identify previously unrecognized subunits and specific interaction partners. Moreover, our biochemical studies shed light on a possible function of the newly identified TIM23-AAC supercomplex. To achieve efficient import and sorting of presequence-carrying preproteins to different mitochondrial compartments, the TIM23 complex relies on the coupling to different energy-converting machineries, like the ATP-driven motor PAM and respiratory chain complexes. Under conditions of low respiratory activity, AAC mediates the import of ATP into mitochondria from the cytosol in exchange with ADP. This process is necessary to maintain matrix ATP levels that are sufficient to fuel ATP-dependent molecular machines like PAM and, additionally, contributes to the generation of $\Delta\psi$. This becomes most obvious in *rho*− mitochondria, where AAC activity is required for preprotein import (52). We propose that both direct ATP supply to the PAM machinery and the efficient use of $\Delta\psi$ for preprotein import may be facilitated by the direct physical coupling of AAC to TIM23 under conditions of net ATP import into mitochondria from the cytosol (*rho*−, fermentative growth, and oxygen limitation). This view is supported by our analysis of *tim17-11* mutant mitochondria that show reduced TIM23-AAC association. Preprotein import into isolated *tim17-11* mitochondria is selectively defective under conditions that render the import reaction sensitive to inhibition of AAC activity. A similar mechanism of local energetic coupling has been demonstrated for the association of $TIM23^{SORT}$ with $\Delta\psi$-generating respiratory chain supercomplexes in respiring cells that supports the $\Delta\psi$-dependent step of preprotein insertion into the inner membrane (21).

In summary, this study identifies the mitochondrial ADP/ATP carrier as a partner protein of the presequence translocase of the inner mitochondrial membrane. Our findings reinforce the view that the TIM23 complex is embedded into an intricate protein network in the inner mitochondrial membrane. The partner proteins of TIM23 support the preprotein import reaction at different stages and under specific physiological conditions.

*Acknowledgments—We thank Drs. Nikolaus Pfanner and Maria Bohnert for discussions and critical reading of the manuscript and Inge Perschil for expert technical assistance.*

## REFERENCES

1. Gilkerson R. W., Selker, J. M., and Capaldi, R. A. (2003) The cristal membrane of mitochondria is the principal site of oxidative phosphorylation. *FEBS Lett.* **546,** 355–358
2. Vogel, F., Bornhövd, C., Neupert, W., and Reichert, A. S. (2006) Dynamic subcompartmentalization of the mitochondrial inner membrane. *J. Cell Biol.* **175,** 237–247
3. Wurm, C. A., and Jakobs, S. (2006) Differential protein distributions define two sub-compartments of the mitochondrial inner membrane in yeast. *FEBS Lett.* **580,** 5628–5634
4. Stuart, R. A. (2008) Supercomplex organization of the oxidative phosphorylation enzymes in yeast mitochondria. *J. Bioenerg. Biomembr.* **40,** 411–417
5. Wittig, I., and Schägger, H. (2009) Supramolecular organization of ATP synthase and respiratory chain in mitochondrial membranes. *Biochim. Biophys. Acta* **1787,** 672–680
6. Palmieri, L., Lasorsa, F. M., Vozza, A., Agrimi, G., Fiermonte, G., Runswick, M. J., Walker, J. E., and Palmieri, F. (2000) Identification and functions of new transporters in yeast mitochondria. *Biochim. Biophys. Acta* **1459,** 363–369
7. Ferramosca, A., and Zara, V. (2013) Biogenesis of mitochondrial carrier proteins: molecular mechanisms of import into mitochondria. *Biochim. Biophys. Acta* **1833,** 494–502
8. Nury, H., Dahout-Gonzalez, C., Trézéguet, V., Lauquin, G. J., Brandolin, G., and Pebay-Peyroula, E. (2006) Relations between structure and function of the mitochondrial ADP/ATP carrier. *Annu. Rev. Biochem.* **75,** 713–741
9. Klingenberg, M. (2008) The ADP and ATP transport in mitochondria and its carrier. *Biochim. Biophys. Acta* **1778,** 1978–2021
10. Kunji, E. R., and Crichton, P. G. (2010) Mitochondrial carriers function as monomers. *Biochim. Biophys. Acta* **1797,** 817–831
11. Traba, J., Satrústegui, J., and del Arco, A. (2009) Transport of adenine nucleotides in the mitochondria of *Saccharomyces cerevisiae*: interactions between the ADP/ATP carriers and the ATP-Mg/Pi carrier. *Mitochondrion* **9,** 79–85
12. Habib, S. J., Neupert, W., and Rapaport, D. (2007) Analysis and prediction of mitochondrial targeting signals. *Methods Cell Biol.* **80,** 761–781
13. Vögtle, F. N., Wortelkamp, S., Zahedi, R. P., Becker, D., Leidhold, C., Gevaert, K., Kellermann, J., Voos, W., Sickmann, A., Pfanner, N., and Meisinger, C. (2009) Global analysis of the mitochondrial N-proteome identifies a processing peptidase critical for protein stability. *Cell* **139,**

428–439
14. Dolezal, P., Likic, V., Tachezy, J., and Lithgow, T. (2006) Evolution of the molecular machines for protein import into mitochondria. *Science* **313,** 314–318
15. Chacinska, A., Koehler, C. M., Milenkovic, D., Lithgow, T., and Pfanner, N. (2009) Importing mitochondrial proteins: machineries and mechanisms. *Cell* **138,** 628–644
16. Endo, T., and Yamano, K. (2009) Multiple pathways for mitochondrial protein traffic. *Biol. Chem.* **390,** 723–730
17. Mokranjac, D., and Neupert, W. (2010) The many faces of the mitochondrial TIM23 complex. *Biochim. Biophys. Acta* **1797,** 1045–1054
18. Dudek, J., Rehling, P., and van der Laan, M. (2013) Mitochondrial protein import: common principles and physiological networks. *Biochim. Biophys. Acta* **1833,** 274–285
19. Chacinska, A., Lind, M., Frazier, A. E., Dudek, J., Meisinger, C., Geissler, A., Sickmann, A., Meyer, H. E., Truscott, K. N., Guiard, B., Pfanner, N., and Rehling, P. (2005) Mitochondrial presequence translocase: switching between TOM tethering and motor recruitment involves Tim21 and Tim17. *Cell* **120,** 817–829
20. Mokranjac, D., Popov-Celeketić, D., Hell, K., and Neupert, W. (2005) Role of Tim21 in mitochondrial translocation contact sites. *J. Biol. Chem.* **280,** 23437–23440
21. van der Laan, M., Wiedemann, N., Mick, D. U., Guiard, B., Rehling, P., and Pfanner, N. (2006) A role for Tim21 in membrane-potential-dependent preprotein sorting in mitochondria. *Curr. Biol.* **16,** 2271–2276
22. Wiedemann, N., van der Laan, M., Hutu, D. P., Rehling, P., and Pfanner, N. (2007) Sorting switch of mitochondrial presequence translocase involves coupling of motor module to respiratory chain. *J. Cell Biol.* **179,** 1115–1122
23. Saddar, S., Dienhart, M. K., and Stuart, R. A. (2008) The $F_1F_o$-ATP synthase complex influences the assembly state of the cytochrome $bc_1$-cytochrome oxidase supercomplex and its association with the TIM23 machinery. *J. Biol. Chem.* **283,** 6677–6686
24. Dienhart, M. K., and Stuart, R. A. (2008) The yeast Aac2 protein exists in physical association with the cytochrome $bc_1$-COX supercomplex and the TIM23 machinery. *Mol. Biol. Cell* **19,** 3934–3943
25. Gebert, M., Schrempp, S. G., Mehnert, C. S., Heißwolf, A. K., Oeljeklaus, S., Ieva, R., Bohnert, M., von der Malsburg, K., Wiese, S., Kleinschroth, T., Hunte, C., Meyer, H. E., Haferkamp, I., Guiard, B., Warscheid, B., Pfanner, N., and van der Laan, M. (2012) Mgr2 promotes coupling of the mitochondrial presequence translocase to partner complexes. *J. Cell Biol.* **197,** 595–604
26. Ieva, R., Heißwolf, A. K., Gebert, M., Vögtle, F. N., Wollweber, F., Mehnert, C. S., Oeljeklaus, S., Warscheid, B., Meisinger, C., van der Laan, M., and Pfanner, N. (2013) Mitochondrial inner membrane protease promotes assembly of presequence translocase by removing a carboxy-terminal targeting sequence. *Nat. Commun.* **4,** 2853
27. van der Laan, M., Meinecke, M., Dudek, J., Hutu, D. P., Lind, M., Perschil, I., Guiard, B., Wagner, R., Pfanner, N., and Rehling, P. (2007) Motor-free mitochondrial presequence translocase drives membrane integration of preproteins. *Nat. Cell Biol.* **9,** 1152–1159
28. Reif, S., Randelj, O., Domanska, G., Dian, E. A., Krimmer, T., Motz, C., and Rassow, J. (2005) Conserved mechanism of Oxa1 insertion into the mitochondrial inner membrane. *J. Mol. Biol.* **354,** 520–528
29. Bohnert, M., Rehling, P., Guiard, B., Herrmann, J. M., Pfanner, N., and van der Laan, M. (2010) Cooperation of stop-transfer and conservative sorting mechanisms in mitochondrial protein transport. *Curr. Biol.* **20,** 1227–1232
30. Stoldt, S., Wenzel, D., Hildenbeutel, M., Wurm, C. A., Herrmann, J. M., and Jakobs, S. (2012) The inner-mitochondrial distribution of Oxa1 depends on the growth conditions and on the availability of substrates. *Mol. Biol. Cell* **23,** 2292–2301
31. Geissler, A., Chacinska, A., Truscott, K. N., Wiedemann, N., Brandner, K., Sickmann, A., Meyer, H. E., Meisinger, C., Pfanner, N., and Rehling, P. (2002) The mitochondrial presequence translocase: an essential role of Tim50 in directing preproteins to the import channel. *Cell* **111,** 507–518
32. Stuart, R. A. (2009) Supercomplex organization of the yeast respiratory chain complexes and the ADP/ATP carrier proteins. *Methods Enzymol.* **456,** 191–208
33. Hutu, D. P., Guiard, B., Chacinska, A., Becker, D., Pfanner, N., Rehling, P., and van der Laan, M. (2008) Mitochondrial protein import motor: differential role of Tim44 in the recruitment of Pam17 and J-complex to the presequence translocase. *Mol. Biol. Cell* **19,** 2642–2649
34. Meisinger, C., Pfanner, N., and Truscott, K. N. (2006) Isolation of yeast mitochondria. *Methods Mol. Biol.* **313,** 33–39
35. Schindelin, J., Arganda-Carreras, I., Frise, E., Kaynig, V., Longair, M., Pietzsch, T., Preibisch, S., Rueden, C., Saalfeld, S., Schmid, B., Tinevez, J.-Y., White, D. J., Hartenstein, V., Eliceiri, K., Tomancak, P., and Cardona, A. (2012) Fiji: an open-source platform for biological image analysis. *Nat. Methods* **9,** 676–682
36. Mick, D. U., Dennerlein, S., Wiese, H., Reinhold, R., Pacheu-Grau, D., Lorenzi, I., Sasarman, F., Weraarpachai, W., Shoubridge, E. A., Warscheid, B., and Rehling, P. (2012) MITRAC links mitochondrial protein translocation to respiratory-chain assembly and translational regulation. *Cell* **151,** 1528–1541
37. Hess, D. C., Myers, C. L., Huttenhower, C., Hibbs, M. A., Hayes, A. P., Paw, J., Clore, J. J., Mendoza, R. M., Luis, B. S., Nislow, C., Giaever, G., Costanzo, M., Troyanskaya, O. G., and Caudy, A. A. (2009) Computationally driven, quantitative experiments discover genes required for mitochondrial biogenesis. *PLoS Genet.* **5,** e1000407
38. Vukotic, M., Oeljeklaus, S., Wiese, S., Vögtle, F. N., Meisinger, C., Meyer, H. E., Zieseniss, A., Katschinski, D. M., Jans, D. C., Jakobs, S., Warscheid, B., Rehling, P., and Deckers, M. (2012) Rcf1 mediates cytochrome oxidase assembly and respirasome formation, revealing heterogeneity of the enzyme complex. *Cell Metab.* **15,** 336–347
39. Pfanner, N., van der Laan, M., Amati, P., Capaldi, R. A., Caudy, A. A., Chacinska, A., Darshi M, Deckers, M., Hoppins, S., Icho, T., Jakobs, S., Ji, J., Kozjak-Pavlovic, V., Meisinger, C., Odgren, P. R., Park, S. K., Rehling, P., Reichert, A. S., Sheikh, M. S., Taylor, S. S., Tsuchida, N., van der Bliek, A. M., van der Klei, I. J., Weissman, J. S., Westermann, B., Zha, J., Neupert, W., and Nunnari, J. (2014) Uniform nomenclature for the mitochondrial contact site and cristae organizing system. *J. Cell Biol.* **204,** 1083–1086
40. Gold, V. A., Ieva, R., Walter, A., Pfanner, N., van der Laan, M., and Kühlbrandt, W. (2014) Visualizing active membrane protein complexes by electron cryotomography. *Nat. Commun.* **5,** 4129
41. Castegna, A., Scarcia, P., Agrimi, G., Palmieri, L., Rottensteiner, H., Spera, I., Germinario, L., and Palmieri, F. (2010) Identification and functional characterization of a novel mitochondrial carrier for citrate and oxoglutarate in *Saccharomyces cerevisiae*. *J. Biol. Chem.* **285,** 17359–17370
42. Rehling, P., Brandner, K., and Pfanner, N. (2004) Mitochondrial import and the twin-pore translocase. *Nat. Rev. Mol. Cell Biol.* **5,** 519–530
43. Claypool, S. M., Oktay, Y., Boontheung, P., Loo, J. A., and Koehler, C. M. (2008) Cardiolipin defines the interactome of the major ADP/ATP carrier protein of the mitochondrial inner membrane. *J. Cell Biol.* **182,** 937–950
44. Chacinska, A., van der Laan, M., Mehnert, C. S., Guiard, B., Mick, D. U., Hutu, D. P., Truscott, K. N., Wiedemann, N., Meisinger, C., Pfanner, N., and Rehling, P. (2010) Distinct forms of mitochondrial TOM-TIM supercomplexes define signal-dependent states of preprotein sorting. *Mol. Cell. Biol.* **30,** 307–318
45. Krayl, M., Lim, J. H., Martin, F., Guiard, B., and Voos, W. (2007) A cooperative action of the ATP-dependent import motor complex and the inner membrane potential drives mitochondrial preprotein import. *Mol. Cell. Biol.* **27,** 411–425
46. Ohlmeier, S., Kastaniotis, A. J., Hiltunen, J. K., and Bergmann, U. (2004) The yeast mitochondrial proteome, a study of fermentative and respiratory growth. *J. Biol. Chem.* **279,** 3956–3979
47. Wachter, C., Schatz, G., and Glick, B. S. (1992) Role of ATP in the intramitochondrial sorting of cytochrome $c_1$ and the adenine nucleotide translocator. *EMBO J.* **11,** 4787–4794
48. Stuart, R. A., Gruhler, A., van der Klei, I., Guiard, B., Koll, H., and Neupert, W. (1994) The requirement of matrix ATP for the import of precursor proteins into the mitochondrial matrix and intermembrane space. *Eur. J. Biochem.* **220,** 9–18

49. Pfanner, N., Tropschug, M., and Neupert, W. (1987) Mitochondrial protein import: nucleoside triphosphates are involved in conferring import-competence to precursors. *Cell* **49,** 815–823
50. Schmidt, O., Harbauer, A. B., Rao, S., Eyrich, B., Zahedi, R. P., Stojanovski, D., Schönfisch, B., Guiard, B., Sickmann, A., Pfanner, N., and Meisinger, C. (2011) Regulation of mitochondrial protein import by cytosolic kinases. *Cell* **144,** 227–239
51. Chacinska, A., Rehling, P., Guiard, B., Frazier A. E., Schulze-Specking, A., Pfanner, N., Voos, W., and Meisinger, C. (2003) Mitochondrial translocation contact sites: separation of dynamic and stabilizing elements in formation of a TOM-TIM-preprotein supercomplex. *EMBO J.* **22,** 5370–5381
52. Giraud, M. F., and Velours, J. (1997) The absence of the mitochondrial ATP synthase δ subunit promotes a slow growth phenotype of *rho-* yeast cells by a lack of assembly of the catalytic sector $F_1$. *Eur. J. Biochem.* **245,** 813–818